Polymer Degradation and Stability 225 (2024) 110784

Contents lists available at ScienceDirect

Polymer Degradation and Stability

journal homepage: www.journals.elsevier.com/polymer-degradation-and-stability

# Ultraviolet C radiation on polypropylene: A potential way to reduce plastic pollution

C. Boronat [a,b,*], V. Correcher [b], J. García-Guinea [c], J.C. Bravo-Yagüe [d]

[a] Department of Inorganic Chemistry, Faculty of Sciences, National University of Distance Education (UNED), Av. de Esparta s/n, Madrid 28232, Spain
[b] Department of Environment, Centre for Energy, Environment and Technology Research (CIEMAT), Av. Complutense 40, Madrid 28040, Spain
[c] Department of Geology, National Museum of Natural Sciences (MNCN), The Spanish National Research Council (CSIC), St. Jose Gutierrez Abascal 2, Madrid 28006, Spain
[d] Department of Analytical Sciences, Faculty of Sciences, National University of Distance Education (UNED), Av. de Esparta s/n, Madrid 28232, Spain

ARTICLE INFO

*Keywords:*
Ultraviolet C radiation
Polypropylene
Plastic pollution reduction
FTIR
Raman
Thermoluminescence

ABSTRACT

This study investigates the application of ultraviolet C (UVC) radiation to extend the lifetime of healthcare items containing polypropylene (PP), particularly personal protective equipment (PPE). The main objectives involve assessing possible PP damage from UVC exposure and detecting UVC treatment within PP samples. FTIR spectroscopy and Raman spectroscopy reveal slight degradation in UVC-irradiated PP samples, demonstrating resilience post-treatment. Investigations using commercial thermoluminescence dosimeters (TLD-100, TLD-200, TLD-400 and GR-200) positioned under varying thicknesses of PP (0.20 and 0.80 mm) identify TLD-100 as a promising UVC detector. Conversely, TLD-200 and TLD-400 do not prove to be effective detectors, exhibiting similar behavior to the dosimeters without a plastic sample. And GR-200 does not possess the capability to differentiate between ionizing and non-ionizing components of UVC radiation. This research emphasizes the role of UVC to prolong the lifetime of healthcare items containing PP, thus aiding in efforts to reduce plastic pollution.

## 1. Introduction

Healthcare materials, such us personal protective equipment (PPE) items, are considered essential worldwide, particularly in reaction to the current COVID-19 (SARS-CoV-2) pandemic [1–6]. Despite its crucial role in preventing infections, the extensive utilization of single-use PPE materials significantly contributes to annual biomedical waste, leading to unintended environmental impacts during widespread use and disposal [1,4,5,7]. This challenge necessitates comprehensive research into the life cycle of PPE items to inform sustainable practices in design, production, reuse and waste management.

The extensive global production of various PPE items, including face masks, hazard suits, gowns and gloves, among others [1–3,5], has used cost-effective polymers such as polypropylene (PP) [3,8,9]. Unfortunately, the subsequent widespread use and inadequate disposal practices, have transformed these essential protective items into an unprecedented source of plastic contamination, especially within aquatic ecosystems [1,3,10,11]. Furthermore, the degradation of PPE items under environmental conditions (i.e. exposure to sea waves and sunlight) has been reported, resulting in the generation of microplastics (MPs), which are described as fragments smaller than 5 mm [1,2,11]. These MPs pose an important ecological threat as they become available to diverse marine organisms, inducing toxic effects that can permeate through the marine food chain [1–3,11]. Moreover, plastic materials has demonstrated the capacity to release toxic chemical additives and serve as a carrier for contaminants, thereby intensifying the overall environmental impact [1,11]. This intricate alteration of plastic materials within aquatic environments underscore the urgency for effective life cycle management, with a specific emphasis on the reuse of these materials, underscoring the broader implications for marine ecosystems [2,11].

In this situation, several disinfection technologies have been suggested for the reutilization of these PPE items [4,7,12]. For example, responding to critical shortages of disposable N95 masks amidst the COVID-19 pandemic, the Centers for Disease Control and Prevention (CDC) have issued guidelines encompassing three distinct procedures aimed at decontaminating and reusing masks: ultraviolet C radiation (UVC), moist heat and vaporous hydrogen peroxide [13]. Specifically, UVC germicidal light, within the wavelength range of 100−280 nm, induces RNA and DNA disruption, leading to the formation of

* Corresponding author.
*E-mail address:* cecilia.boronat@ccia.uned.es (C. Boronat).

https://doi.org/10.1016/j.polymdegradstab.2024.110784
Received 28 March 2024; Received in revised form 18 April 2024; Accepted 22 April 2024
Available online 23 April 2024

pyrimidine dimers and thereby inactivating viruses and various microorganisms [7]. Several studies have demonstrated that applying UVC dosages from 0.5 to 1.8 J·cm$^{-2}$ results in over 99.9 % inactivation for numerous influenza coronaviruses and viruses [14,15]. Furthermore, UVC radiation has the potential to alter chemo-physical attributes of polymers, which can encompass: (i) a decrease in mechanical strength caused by chain scission and *photo-oxidation* process that disrupts chemical bonds; (ii) *radical formation* may cause initiation of degradation and/or polymerization reactions; (iii) *functional groups* could emerge within the polymer structure, leading to alterations in physical and chemical characteristics; (iv) colorants or pigments in the polymer may disintegrate, causing a *yellowing process* and/or *bleaching effect*; (v) *optical properties* may vary, affecting reflectance or transmittance features; and/or (vi) *fatigue resistance* may be reduced, heightening the chance of breakage or malfunction when subjected to repeated loads [6,16]. Moreover, it is fundamental to address at least two key considerations when employing UVC radiation for sterilization purposes in the recycling of PPE materials: (1) evaluating the potential damage that PP materials may incur due to UVC radiation exposure and (2) identifying the existence of UVC radiation using thermoluminescence dosimeters (TLDs) positioned under PP materials. To address these considerations, Fourier transform infrared spectroscopy (FTIR), Raman spectroscopy and thermoluminescence (TL) stand as appropriate techniques for their determination [6].

Thus, FTIR and Raman spectroscopy might serve as invaluable tools for understanding the molecular and structural properties of PP, a commonly used polymer in PPE items especially in face masks [1,3,10,17,18]. Examining the intrinsic vibrations of functional groups within the crystalline lattice of the polymer using FTIR could provide insights into microscopic deformations and potential conformational changes in PP materials. Providing a comprehensive insight into molecular-level structural properties, this non-invasive method eliminates the necessity for any form of physical or chemical sample pretreatment. Additionally, FTIR ensures a thorough evaluation of the composition and robustness of PP materials, confirming their suitability for essential applications [1,3,17–19]. Furthermore, Raman spectroscopy provides insights into the rotational and vibrational energy levels of molecules, making it an equally important complement to FTIR. This technique could prove beneficial in exploring crystallinity, stress and molecular arrangement within PP materials, thereby providing insights into their suitability for reuse. Raman spectroscopy, being highly precise and non-destructive, serves as a technique for evaluating chemo-physical properties of PP materials [10,19].

Despite the numerous advantages demonstrated by UVC radiation, there exists no established method to definitively determine whether a material, especially PP materials used in PPE items, has undergone irradiation. The lack of understanding regarding the interactions between UVC light and complex surfaces is notable, highlighting the urgent necessity for additional research. The intricacies of UVC disinfection technologies for decontaminating these materials present a unique challenge, exacerbated by the limited pre-COVID data on UV disinfection for PPE items. Earlier studies lacked current relevance, employed non-standardized methods, and required updates to align with the demands of the pandemic. The emergency reuse of PPE items during supply chain disruptions prompted an upsurge in investigations assessing the efficacy of UV disinfection for these materials. In spite of the recent introduction of surface-UV exposure products, regulatory guidelines from the National Institute of Standards and Technology (NIST) and U.S. Food and Drug Administration (FDA) remain in their preliminary stages, leaving a void in guidance for best practices in establishing masks disinfection processes [12,20].

This demanded methodology could be grounded in the identification of materials exposed to UV irradiation through discernible alterations in their chemical, physical and biological properties [6,21–23]. Thus, TL might emerge as an exceptionally accurate, appropriate, economical and effective approach for this objective. This technique operates based on the release of photons from a solid dielectric material (insulator or semiconductor), after being exposed to radiation (non-ionizing or ionizing) from natural or artificial sources. Throughout the thermal analysis, the TL signal is captured by a photomultiplier tube and subsequently registered based on temperature or wavelength variations. The *TL curve* or *glow curve*, produced as a result, showcases characteristic luminescent patterns in both shape and intensity, with a direct correlation to the rate of heating and UV dosage [24]. This technique holds considerable potential for identifying UV exposure in reusable materials, ensuring compliance with established safety and quality standards. In addition, several detectors and dosimeters with the capacity to detect and record UVC radiation are available. These devices encompass electronic instruments and synthetic dosimeters with varied compositions, such us, LiF: Ti, Mg (TLD-100), $CaF_2$: Dy (TLD-200), $CaF_2$: Mn (TLD-400) and LiF: Mg, Cu, P (GR-200), among others [23]. For this reason, TL techniques and other methodologies enable the determination of their structures, typomorphic features, compositions, and genic characteristics. These methods attribute various luminescent emissions to surface, structural, intrinsic and extrinsic defects.

This research aims to evaluate the UVC-TL responses of commercial TLDs positioned under PP samples (0.20 and 0.80 mm) of varying thicknesses. Additionally, FTIR and Raman spectroscopy were utilized to characterize PP samples and explore possible structural and chemical changes caused by exposure of UVC radiation. This study not only addresses the technical feasibility of using UVC radiation to extend the lifespan of PP-based PPE items, but also situates this approach within the larger framework of environmental sustainability efforts. By demonstrating the potential for UVC treatment to prolong the usability of PPE materials, it highlights a viable strategy for mitigating the environmental impact of healthcare-related plastic waste. This approach aligns with global efforts to transition towards more sustainable waste management practices, offering a dual benefit of enhancing infection control measures while concurrently reducing the volume of plastic waste generated by healthcare facilities. Thus, these findings contribute to a growing body of knowledge that seeks practical solutions for the dual challenges of public health protection and environmental conservation.

## 2. Materials and methods

This investigation involved the analysis of two PP samples with varying thicknesses, denoted as 0.20 mm (PP 1) and 0.80 mm (PP 2). ATR-FTIR and Raman spectroscopy techniques were employed for the structural and chemical characterization of the materials. PP samples were cleaned using a 70:30 ratio solution of isopropyl alcohol and water, followed by rinsing with distilled water and drying to remove any remaining moisture. Infrared absorption spectra were obtained at room temperature (RT) within 4000 to 400 cm$^{-1}$ utilizing a Spectrum FT-IR-4100 spectrometer. Raman spectra were conducted employing a Thermo Fisher DRX Raman microscope, providing a spatial resolution of 1 μm at RT. The experimental setup was controlled using Spectra Manager® software from JASCO (Japan), with a spectral resolution set at 4 cm$^{-1}$. The confocal microscope employed a 20x objective, and the laser source emitted light at a wavelength of 532 nm with a laser power of 6 mW, operating at full capacity. A spectral resolution of 1.92 cm$^{-1}$ was attained as Raman spectra were recorded in the range of 3500 to 70 cm$^{-1}$. Following data acquisition for both FTIR and Raman spectroscopic techniques, post-measurement processing was conducted, including baseline correction and noise reduction.

Using an automated irradiator developed at CIEMAT [25], the UVC radiation was carried out for one hour at RT. This device facilitated a lamp of TUV-6 W Hg emanating light at 254.7 nm for UV illumination. The UV irradiance level at a distance of 10 cm was measured at 0.03 W·m$^{-2}$. PP samples were stored in a black bag protected from light before and after exposure to UVC irradiation. These storage conditions were upheld in a controlled environment, ensuring regulated temperature and humidity levels. Commercial dosimeters, namely LiF: Ti, Mg

(TLD-100), $CaF_2$: Dy (TLD-200) and $CaF_2$: Mn (TLD-400) were provided by Harshaw Chemical Company (USA), with dimensions of 0.32 × 0.32 × 0.09 $cm^3$ and, LiF: Mg, Cu, P (GR-200) discs from Beijing Shiying Radiation Detector Works (China), measuring 4.5 Ø 0.8 $mm^3$, were placed under PP samples to assess radiation penetration through the plastic during an irradiation treatment. Following exposure to a high temperature of 400 ± 1 °C for one hour in an electrical oven, the TLDs underwent annealing to eliminate any stored information. An automated Risø TL reader model TL DA-12, furnished with an EMI 9635 QA photomultiplier, was utilized to analyze the TL properties of these detectors [26]. For emission analysis, a FIB002-blue filter with a peak wavelength range of 320 – 480 nm (FWHM of 80 ± 16 nm and transmittance of 60 %) was employed. The TL reader was equipped with a $^{90}Sr$ / $^{90}Y$ source emitting radiation at a dose rate of 0.011 $Gy{\cdot}s^{-1}$, calibrated using a photon source containing $^{137}Cs$ in a secondary standard laboratory [27]. To ensure reliable measurements, all TL readings were conducted with a linear heating rate of 5 °C·$s^{-1}$, spanning from RT up to 400 °C, within a $N_2$ atmosphere. Background signals originating from incandescence and detector noise were removed from the TL data subsequent to a second TL readout of the dosimeters, aimed at their determination.

## 3. Results and discussion

### 3.1. Investigating possible PP degradation: insights from FTIR analysis

The possible degradation of PP samples due to UVC radiation was carried out in films of 0.20 and 0.80 thicknesses. This variable could potentially have an influence on the effectiveness of UVC irradiation on this polymer, emphasizing the importance of measuring its impact on preserving sterility and material integrity. PP is a versatile thermoplastic polymer created from the monomer propylene, a hydrocarbon with the chemical formula $(C_3H_6)_n$ and synthesized via chain-growth polymerization. This process generates long chains, as illustrated in Fig. 1a:

UVC radiation has the potential to initiate a *photo-oxidative degradation* mechanism in PP material, as depicted in Fig. 1b. This process involves an initial decomposition reaction wherein alkyl radicals are generated from polymer macromolecules, resulting in the fragmentation of PP chains through mechanisms such as C–H scissions (refer to reaction [1] of Fig. 1b). Subsequently, a propagation step ensues, generating free radicals, including peroxy (−O−O•) and hydroperoxide radicals (−O−OH), which might decompose, yielding alkoxy radicals. These radicals can either extract hydrogen from the polymeric backbone or experience β-scission (refer to reaction [2] of Fig. 1b). The termination step leads to the degradation of the polymer matrix due to the formation of diverse carbonyl species (refer to reaction [3] of Fig. 1b). This degradation could result in a reduction in molecular weight, thereby compromising the mechanical and tensile properties of the PP material [29–31].

The extensive investigation into the *photo-degradation* and *photo-oxidative degradation* processes of PP material is evident in numerous studies [30–32]. The process of *photo-degradation* can take place even in the absence of oxygen, leading to either cross-linking or chain breaking, and also in an oxygen-rich environment, resulting in *photo-oxidative degradation*. UV radiation, in conjunction with various catalysts either alone or in combination, can induce this process, often accelerated at elevated temperatures. Additionally, exposure of PP material to UV radiation in an aerated environment induces *photo-degradation*, causing effects such as *yellowing, bleaching*, gradual embrittlement, cross-linking and chain scission due to oxidation [29,32]. The *yellow discoloration* resulting from PP aging, especially when exposed to outdoors conditions, is an important adverse effect [29]. This process may involve the generation of hydroperoxide (−O−OH) and peroxy (−O−O•) radicals, leading to the disintegration of an allyl radical ($C_3H_5$ •) and resulting in the subsequent formation of carbonyl compounds (C=O) [28,29,31,32].

Offering valuable insights into the molecular alterations within the plastic material, FTIR spectroscopy enables the elucidation of the emergence of new chemical bonds and functional groups among the *photo-oxidative degradation* of PP samples. To achieve this objective, an analysis of ATR-FTIR spectra was conducted from 4000 to 400 $cm^{-1}$. The standard procedure was adhered to, with transmission (in %) plotted in relation to wavenumber (in $cm^{-1}$). Thus, non-irradiated PP samples were compared with those exposed to 1-hour UVC irradiation, as presented in Fig. 2 (a and b). The identified ATR-FTIR bands are

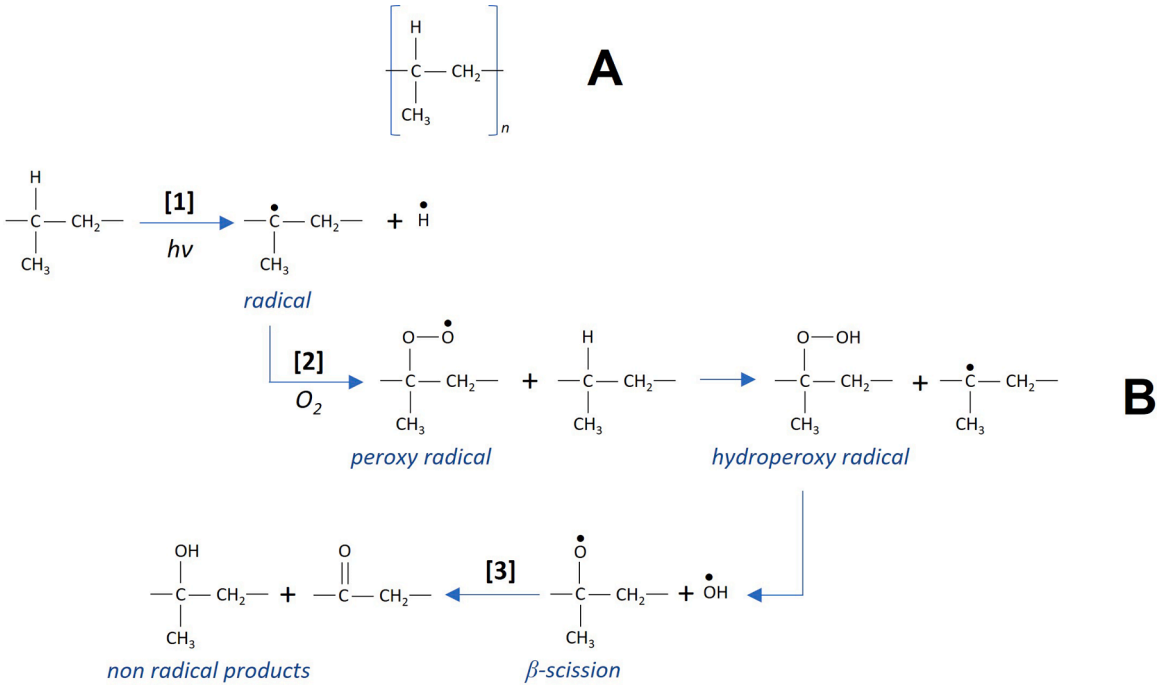


**Fig. 1.** (A) Polypropylene $(C_3H_6)_n$ molecular structure, composed of repeating units formed through the polymerization of propylene. And (B) *photo-oxidative degradation* of polypropylene characterized by radical processes denoted as [1]-initiation, [2]-propagation and [3]-termination steps (Figure adapted from [28,29]).

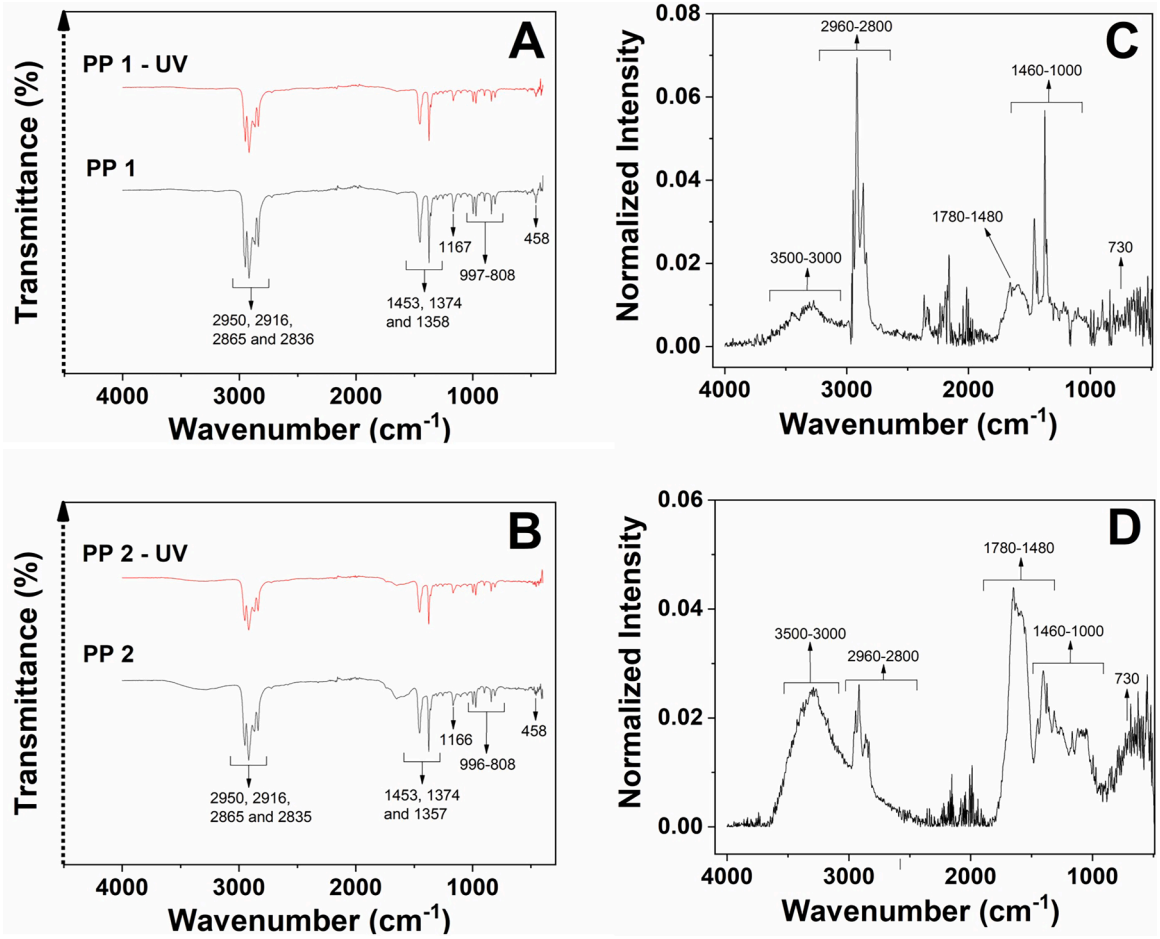


**Fig. 2.** ATR-FTIR spectra (1st column) and normalized ATR-FTIR spectra (2nd column) of polypropylene samples. The 1st line represents PP 1 (0.20 mm), while the 2nd line corresponds to PP 2 (0.80 mm). The spectra depict both unexposed and UVC-exposed conditions. Adjustments have been made to the signal of the UVC-exposed PP samples to avoid spectral overlapping.

detailed in Table 1, while the response, normalized and displayed in Fig. 2 (C and D), unveils potential disparities in the signal after the UVC exposure.

The current infrared absorption spectrum clearly shows the distinctive ATR-FTIR peaks, as presented in Fig. 2 (a and b). These peaks offer valuable information about the bonding strength within the polymer, as further explained. It is important to recognize that while the ATR-FTIR spectra suggest the impact on various bonds in the sample is nearly negligible, other research has suggested that these changes in bond strength become increasingly noticeable with extended periods of irradiation [33].

**Table 1**
Vibrational modes associated with observed ATR-FTIR bands in polypropylene materials. Where, b: backbone; δ: bending; ν: stretching; ρ: rocking; ω: wagging; sym.: symmetric and asym.: asymmetric.

| Wavenumber ($cm^{-1}$) | Vibrational modes |
|---|---|
| 2950 | $\nu CH_3$ asym. |
| 2916 | $\nu CH_2$ asym. |
| 2865 | $\nu CH_2$ sym. |
| 2836 | $\nu CH_2$ sym. |
| 1453 | $\delta CH_3$ asym. and $\delta CH_2$ |
| 1374 | $\delta CH_3$ sym., $\omega CH_2$, $\delta CH$ and $\nu C{-}C_b$ |
| 1358 | $\delta CH_3$ sym. and $\delta CH$ |
| 1167 | $\nu C{-}C_b$, $\rho CH_3$ and $\delta CH$ |
| 997 | $\rho CH_3$, $\delta CH$ and $\omega CH_2$ |
| 972 | $\rho CH_3$ and $\nu C{-}C_b$ |
| 897 | $\rho CH_3$, $\rho CH_2$ and $\delta CH$ |
| 840 | $\rho CH_2$, $\nu C{-}C_b$, $\nu C{-}CH_3$ and $\rho CH_3$ |
| 808 | $\rho CH_2$, $\nu C{-}C_b$, $\nu C{-}CH_3$ and $\rho CH_3$ |
| 458 | $\omega CH_2$ |

Hence, the ATR-FTIR spectrum of the PP samples, as depicted Fig. 2 (a and b), exhibits discernible peaks at characteristic wavenumbers, each associated with particular molecular vibrations: (i) firstly, peaks at 2950 and 2916 $cm^{-1}$ can be ascribed to $\nu CH_3$ asym. and $\nu CH_2$ asym. vibrations, respectively; (ii) secondly, peaks at 2865 and 2836 $cm^{-1}$ could correspond to $\nu CH_2$ sym. vibrations. Additionally, (iii) peaks are observed at 1453, 1374 and 1358 $cm^{-1}$ could be linked to different $\delta CH_3$ asym., $\delta CH_2$, $\delta CH_3$ sym., $\omega CH_2$, $\delta CH$ and $\nu C{-}C_b$ vibrations. Furthermore, (iv) peak at 1167 $cm^{-1}$ could be attributed with $\nu C{-}C_b$, $\rho CH_3$ and $\delta CH$ vibrations. Moving forward, (v) peak at 997 $cm^{-1}$ could be related to $\rho CH_3$, $\delta CH$ and $\omega CH_2$ vibrations. Subsequently, (vi) peak at 972 $cm^{-1}$ could be indicative of $\rho CH_3$ and $\nu C{-}C_b$ vibrations. Moreover, (vii) peak at 897 $cm^{-1}$ could be linked to $\rho CH_3$, $\rho CH_2$ and $\delta CH$ vibrations. Finally, (viii) peaks at 840 and 808 $cm^{-1}$ correspond to $\rho CH_2$, $\nu C{-}C_b$, $\nu C{-}CH_3$ and $\rho CH_3$ vibrations, while (ix) peak at 458 $cm^{-1}$ could be due to $\omega CH_2$ vibrations [1,3,17,34–38].

The normalized ATR-FTIR spectra of both unexposed (Fig. 2c) and UVC-exposed PP samples (Fig. 2d), exhibited negligible variances of less than 7 % (PP 1) and 4 % (PP 2) in transmittance relative to the average value following UVC treatment. Signifying their resistance to further degradation, this finding highlights the robustness of the bands in PP ATR-FTIR spectra under UVC radiation. However, to assess the *photo-oxidative degradation* process, the focus lies on two regions within the infrared spectrum, specifically pertaining to the stretching vibrations of hydroxyl (O–H) and carbonyl (C=O) groups. The intensity of

these groups could increase upon the exposure time and this behavior serves as an indicator of the material degradation [30]. Thus, the possible alterations observed in the ATR-FTIR spectra of PP samples upon exposure to UVC irradiation include:

(i) In the hydroxyl (O–H) region, the broad band ranging from 3500 to 3000 $cm^{-1}$ comprises the $\nu$O–H vibrations of alcohols and hydroperoxides. A minor contribution from the O–H absorption of carboxylic acids is present due to the *photo-oxidative degradation* process [3,30].
(ii) Possible breakage of C–H bonds within the polymer chain leads to alterations in the intensity and position of $\nu CH_3$ asym., $\nu CH_2$ asym. and $\nu CH_2$ sym. bands typically located in the 2960−2800 $cm^{-1}$ region [34,35,37].
(iii) Within the carbonyl (C=O) region, which peaks at 1780−1480 $cm^{-1}$, the band configuration suggests the presence of multiple functional groups, including the carbonyl group of carboxylic acids in a dimeric state, carbonyl groups of esters, or the carbonyl vibration of carboxylic acids associated with hydroxyl groups and/or the formation of γ-lactones [28,30]. These changes could result from the *photo-oxidative degradation* of polymer chains.
(iv) Bands associated with δC-H vibrations in the 1460−1000 $cm^{-1}$ region may undergo changes due to UVC irradiation and the potential generation of new functional groups [34,35,37].
(v) Finally, UVC radiation can impact the crystalline structure of PP material, leading to changes in bands associated with crystalline structure, such as those in the 730 $cm^{-1}$ region [36].

Upon analysis of the normalized ATR-FTIR spectra for the PP samples in Fig. 2 (C and D), subtle alterations in the characteristic bands were discernible, indicating minimal changes associated with a *photo-oxidative degradation* process affecting its molecular structure (< 7 % transmittance relative). To summarize, these conducted measurements provide evidence indicating that none of the PP samples undergoes degradation following treatment with UVC irradiation, as suggested by these findings. The slight variations observed seem to be inherent to the properties of PP, including its polymer molecular mass distribution, crystalline structure, additives, among others. Additionally, these differences might be linked to the individual histories of the samples, such as manufacturing processes, previous environmental contact and conditions for storage, rather than being solely influenced by UVC radiation.

### 3.2. *Investigating possible PP degradation: Raman spectroscopy findings*

In conjunction with ATR-FTIR analysis (Fig. 2), we have employed Raman spectroscopy (Fig. 3) to characterize the PP samples with varying thicknesses. This technique could act as a supplementary method to furnish a more thorough and in-depth comprehension of potential structural and chemical alterations in PP materials. Fig. 3 (a and b) showcases a comparative analysis of Raman spectra for polypropylene (PP) samples, both unexposed and subjected to 1 h of UVC radiation. The Raman spectra were generated by plotting the intensity (in cps) in relation to the Raman shift (in $cm^{-1}$), adhering to the standard methodology. These spectra unveil distinctive features indicative of the vibrational modes associated with functional groups and molecules. Moreover, Fig. 3 (c and d) illustrates the normalized response, offering

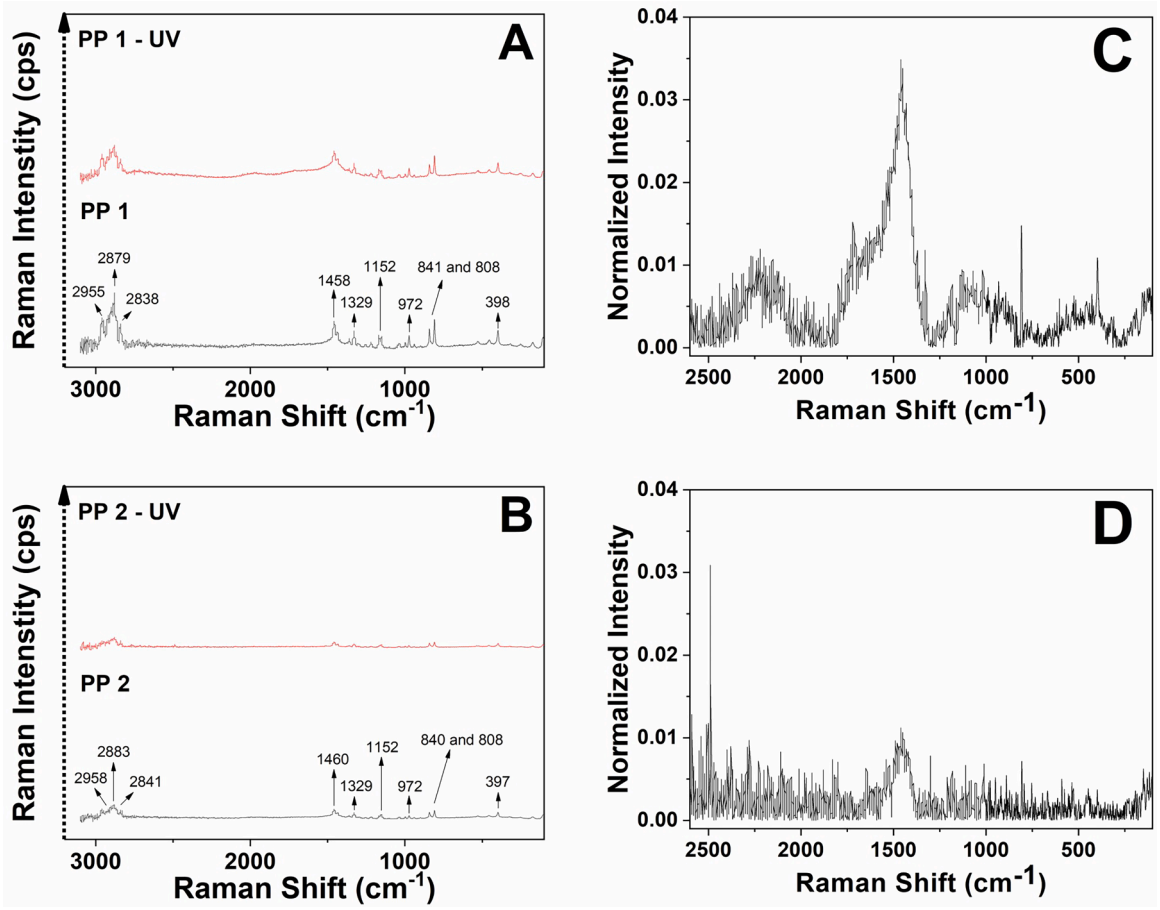


**Fig. 3.** Raman spectra (1st column) and normalized Raman spectra (2nd column) of polypropylene samples. The 1st line represents PP 1 (0.20 mm), while the 2nd line corresponds to PP 2 (0.80 mm). The spectra depict both unexposed and UVC-exposed conditions. Adjustments have been made to the signal of the UVC- exposed PP samples to avoid spectral overlapping.

insights into the possible alterations post UVC treatment. The Raman bands are detailed in Table 2. In Fig. 3 (a and b), unexposed PP materials display distinctive bands corresponding to the vibrational modes inherent to PP molecules [19,34,35].

Prominent bands peak at: (i) 2955, 2879 and 2838 $cm^{-1}$, linked to $\nu CH_3$ asym., $\nu CH_3$ sym. and $\nu CH_2$ sym. vibrations; (ii) 1458 $cm^{-1}$, which correspond to $\delta CH_3$ asym. and $\delta CH_2$ vibrations; (iii) 1329 $cm^{-1}$, associated with δCH and $\tau CH_2$ vibrations; (iv) 1152 $cm^{-1}$, related to $\nu CC_b$, $\nu C—CH_3$, δCH and $\rho CH_3$ vibrations; (v) 972 $cm^{-1}$, corresponding to $\rho CH_3$ and $\nu CC_b$ vibrations; (vi) 841 and 808 $cm^{-1}$, due to $\rho CH_2$, $\nu CC_b$, $\nu C—CH_3$ and $\rho CH_3$ vibrations; and (vii) 398 $cm^{-1}$, linked to $\omega CH_2$ and δCH vibrations [19,34,35].

An inverse relationship between the thickness of the PP samples and the Raman signal intensity is evident from the results. Particularly noteworthy is the increase in Raman intensity value as the sample thickness decreases (i.e., PP 1 with a thickness of 0.20 mm), reaching approximately 60 cps at 800 $cm^{-1}$, contrasting with the PP 2 sample with approximately 15 cps. The measured Raman signal intensity experiences a decline, attributed to the occurrence of Raman shielding, which primarily hinges on the thickness of the sample. This decrease results from scattering and light absorption phenomena affected by the arrangement, constitution and thickness of the sample [39]. Notably, regardless of thickness, non-irradiated PP samples exhibit consistent Raman bands that align with the characteristic spectrum of the PP molecule [34,35].

However, it is essential to recognize that the position and intensity of these Raman bands may vary based on diverse factors, such as polymer molecular mass distribution, degree of crystallinity and/or manufacturing production, among others [40]. For example, PP characterized by a heightened crystallinity degree might display more prominent Raman bands due to the elevated PP molecule concentration and an elevated polymer chain configuration structural level [41]. Thus, PP can manifest in two distinct structural forms [8,18]: (1) *isotactic PP* form, where the methyl ($-CH_3$) groups in the monomer units align on the polymer chain. This uniformity creates an ordered and symmetrical structure, contributing to its relatively high crystallinity and mechanical strength. And (2) *atactic PP* form exhibits randomly distributed methyl groups ($-CH_3$) along the polymer chain, giving rise an unordered and amorphous structure. Therefore, in the isotactic PP form, several distinct bands are detected within the 1350−800 $cm^{-1}$ [19]. In contrast, the spectra of the atactic PP form notably differs, characterized by broader bands, and the disappearance of these distinct sharp bands, except for those near 1155 $cm^{-1}$ and 970 $cm^{-1}$ [19]. For such reason, one might presume that both PP samples utilized in this study could showcase the atactic PP form, resulting in an unordered and amorphous structure, indicated by the broader Raman bands lacking distinct sharp peaks, except for those centered at 1152 and 972 $cm^{-1}$.

**Table 2**
Vibrational modes corresponding to the observed Raman bands in polypropylene materials. Where, b: backbone; δ: bending; ν: stretching; ρ: rocking; τ: twisting; ω: wagging; sym.: symmetric and asym.: asymmetric.

| Wavenumber ($cm^{-1}$) | | | | |
|---|---|---|---|---|
| Unexposed | | UVC-exposed | | Vibrational modes |
| PP 1 | PP 2 | PP 1 | PP 2 | |
| 2955 | 2958 | 2956 | – | $\nu CH_3$ asym. |
| 2879 | 2883 | 2878 | 2878 | $\nu CH_3$ sym. |
| 2838 | 2841 | 2834 | – | $\nu CH_2$ sym. |
| 1458 | 1460 | 1459 | 1459 | $\delta CH_3$ asym. and $\delta CH_2$ |
| 1435 | 1435 | 1431 | 1435 | $\delta CH_3$ asym. |
| 1360 | 1359 | 1359 | 1360 | $\delta CH_3$ sym. and δCH |
| 1329 | 1329 | 1329 | 1329 | δCH and $\tau CH_2$ |
| 1297 | – | – | 1297 | $\omega CH_2$, δCH and $\tau CH_2$ |
| 1249 | 1255 | 1251 | – | δCH, $\tau CH_2$ and $\rho CH_3$ |
| 1220 | 1219 | 1219 | 1220 | $\tau CH_2$, δCH and $\nu CC_b$ |
| 1168 | 1167 | 1168 | 1165 | $\nu CC_b$, $\rho CH_3$ and δCH |
| 1152 | 1152 | 1148 | 1152 | $\nu CC_b$, $\nu C$-$CH_3$, δCH and $\rho CH_3$ |
| – | 1101 | – | – | $\nu CC_b$, $\rho CH_3$, $\omega CH_2$, τCH and δCH |
| 1036 | 1037 | 1038 | 1036 | $\nu C$-$CH_3$, $\nu CC_b$ and δCH |
| 997 | 997 | 999 | 992 | $\rho CH_3$, δCH and $\omega CH_2$ |
| 972 | 972 | 972 | 973 | $\rho CH_3$ and $\nu CC_b$ |
| 940 | 940 | 937 | 934 | $\rho CH_3$ and $\nu CC_b$ |
| – | 900 | – | 900 | $\rho CH_3$, $\rho CH_2$ and δCH |
| 841 | 840 | 840 | 840 | $\rho CH_2$, $\nu CC_b$, $\nu C$-$CH_3$ and $\rho CH_3$ |
| 808 | 808 | 808 | 808 | $\rho CH_2$, $\nu CC_b$, $\nu C$-$CH_3$ and $\rho CH_3$ |
| 524 | 530 | 525 | 535 | $\omega CH_2$, $\nu C$-$CH_3$ and $\rho CH_2$ |
| 454 | 455 | 454 | 455 | $\omega CH_2$ |
| 398 | 397 | 398 | 397 | $\omega CH_2$ and δCH |
| 314 | 321 | 314 | 318 | $\omega CH_2$ |
| 249 | 249 | 249 | 253 | $\omega CH_2$ and δCH |

Additionally, environmental factors, such as temperature fluctuations, sunlight and chemical treatments (i.e., pigments, additives and antioxidants), along with exposure to UV radiation can cause variations in the Raman spectrum of PP materials. As previously mentioned, UVC radiation has the capacity to initiate a *photo-oxidative degradation* process in PP materials, giving rise the rupture of polymer chains (specifically, C–H bonds), the creation of free radicals (peroxy, hydroperoxide and allyl radicals), following creation of carbonyl compounds (C=O), and a reduction in the molecular mass of the polymer. Other studies have also noted loss of flexibility and embrittlement in PP samples due to this *photo-oxidative degradation* process [10]. Therefore, extensive research is necessary to investigate these reactions, elucidate the dispersion patterns of free radicals and examine the physicochemical attributes of plastic samples exposed to UVC irradiation [10,28–32].

As depicted in Fig. 3 (a and b), the Raman spectra of PP samples exposed to UVC radiation exhibit comparable patterns to those observed in the unexposed samples. This underscores the stability of these specific Raman bands under UVC exposure, affirming their resilience against additional degradation, aligning with the conclusions drawn from the ATR-FTIR analysis. Thus, the observed possible alterations in the Raman spectra of PP samples following exposure to UVC irradiation are as follows:

(i) Both PP samples displayed a slight reduction in the intensity of their distinctive peaks, in line with prior research findings [10,16].
(ii) Analysis of the normalized Raman spectrum for PP 1 sample after UVC irradiation in Fig. 3C, reveals minor changes in the distinctive bands, indicating subtle modifications in its molecular structure (less than < 4 %). A minor increase in Raman signal intensity at 1460 $cm^{-1}$ might indicate heightened $\delta CH_3$ asym. and $\delta CH_2$ vibrations [19]. Additionally, the decreased Raman signal intensity at 1720 $cm^{-1}$ could be linked to the presence of a mixture of hydroperoxide groups, where ketones absorb near 1720 $cm^{-1}$, aldehydes near 1735 $cm^{-1}$, and carboxylic acids near 1710 $cm^{-1}$ [19].
(iii) The normalized Raman spectrum for PP 2 sample (Fig. 3D) exhibits minimal alteration (less than < 1 %), suggesting no discernible evidence of polymer chain degradation under UVC treatment.

In summary, these observations suggest that neither PP sample exhibited degradation after UVC irradiation exposure, as indicated by the measurements conducted. As revealed by the ATR-FTIR analysis, the slight disparities seem inherent to the properties of the PP materials, encompassing factors such as weight distribution, crystalline structure, additives, and various other aspects, or may be linked to their histories, such us previous environmental contact, conditions for storage and manufacturing production, among others, instead of being attributed to UVC irradiation. While these findings indicate a promising application of UVC radiation for extending the lifespan of PP-based PPE items, there are several practical considerations and limitations that warrant discussion. Firstly, the effectiveness of UVC treatment can vary based on the intensity of the radiation and the duration of exposure, factors that require careful optimization to avoid material degradation while

ensuring disinfection efficacy. Additionally, the scalability of UVC treatment in healthcare settings poses a challenge, given the need for specialized equipment and safety protocols to mitigate personal exposure risks. Furthermore, the long-term effects of repeated UVC treatments on the structural integrity of PP materials remain to be fully understood. These limitations highlight the need for further research to refine UVC treatment protocols and to evaluate their feasibility and safety in high-throughput healthcare environments.

### 3.3. Detecting UVC treatment in PP samples: a comparative study of the UVC-TL emissions in commercial dosimeters

The examination of shielding PP materials from UVC radiation denotes a relevant endeavor aimed at accurately assessing potential radiation exposure. This comparative study on UVC-TL emission, for the purpose of detecting UVC radiation output with varying thicknesses of PP samples, has utilized various commercial dosimeters [23]. These include TLD-100 (LiF: Ti, Mg), TLD-200 ($CaF_2$: Dy), TLD-400 ($CaF_2$: Mn) and GR-200 (LiF: Mg, Cu, P). This methodology facilitates a qualitative differentiation between unexposed and UVC-exposed PP materials, guaranteeing their safety and efficacy for diverse uses. Moreover, characterization utilizing ATR-FTIR and Raman spectroscopy, as previously outlined, exhibited no discernible degradation subsequent to UVC radiation, thus ensuring the resilience of the PP samples under the specified experimental settings. Fig. 4 displays the TL emissions resulting from UVC radiation exposure of the PP samples, detected using commercial TLDs materials. Each emission offers insights into the intrinsic characteristics governing the interplay between UVC radiation and these TLDs, depending on the thickness of the PP sample.

### 3.4. TLD-100 (LiF: Ti, Mg) TL emission study under UVC radiation

Distinct dual components of TL emissions caused by UVC radiation from this commercial dosimeter under PP materials are evident in Fig. 4 (A and B). Initially, up to approximately 250 °C, the TL glow displays prominent peaks at around 150 °C, 190 °C and 230 °C. These observed peaks are thought to originate from the ionizing component, likely as a result of the generation of defect complexes involving $Mg^{2+}$ vacancies and $Ti^{4+}$–$OH^-$, known as Mg-dipoles. Furthermore, they may involve $Ti^{4+}$–$OH^-$/$Mg^{2+}$-trimer structures and/or $Mg^{2+}$dipoles [42]. Previous research has established the existence of hydroxyl ions ($OH^-$) within the crystalline structure of the TLD-100 material, which is composed of LiF. This presence is indicated by the substitution of $F^-$ ions (1.33 Å) with $OH^-$ ions, which have a slightly larger ionic radius of 1.37 Å. These $OH^-$ groups demonstrate favorable reactivity with metals such as $Ti^{4+}$ and $Mg^{2+}$ions within the TLD-100 material, potentially enhancing TL sensitivity [43]. Subsequently, at higher temperatures beyond approximately 250 °C, TL emission corresponds to the non-ionizing part. In this scenario, a solitary peak of TL emerges at around 300 °C, suggesting an interaction between the TLD-100 dosimeter and the non-ionizing component [23].

Analyzing the intensity ratios among these dual components, the ratios observed for PP 1 (Fig. 4a) and PP 2 (Fig. 4b) are 1:3:5:5 and 1:2:5:2, respectively. Notably, in the PP 1 sample (Fig. 4a), the three particular peaks associated with the ionizing UVC component shift to higher temperatures, with the most significant peak centered at approximately 230 °C. This observation may imply that the PP 1 sample (0.20 mm thickness) selectively absorbs the non-ionizing part, permitting the penetration of the ionizing component. By employing different thicknesses of PP (0.20 and 0.80 mm) in this study, notable disparities in the TL emissions related to the ionizing part may arise, extending to around 250 °C. Moreover, the heightened sensitivity of the PP 1 material (Fig. 4A) to UVC radiation is evident from the peak signal around 300 °C, possibly attributed to the penetrability of the sample with less thickness to the non-ionizing part. In consequence, this commercial dosimeter shows promise as a potential detector of UVC radiation, mostly due to the significant emission detected at around 300 °C, indicative of the non-ionizing part. Under the present measurement conditions, the emission stands out notably in the thinner PP 1 sample, measuring 0.20 mm in thickness.

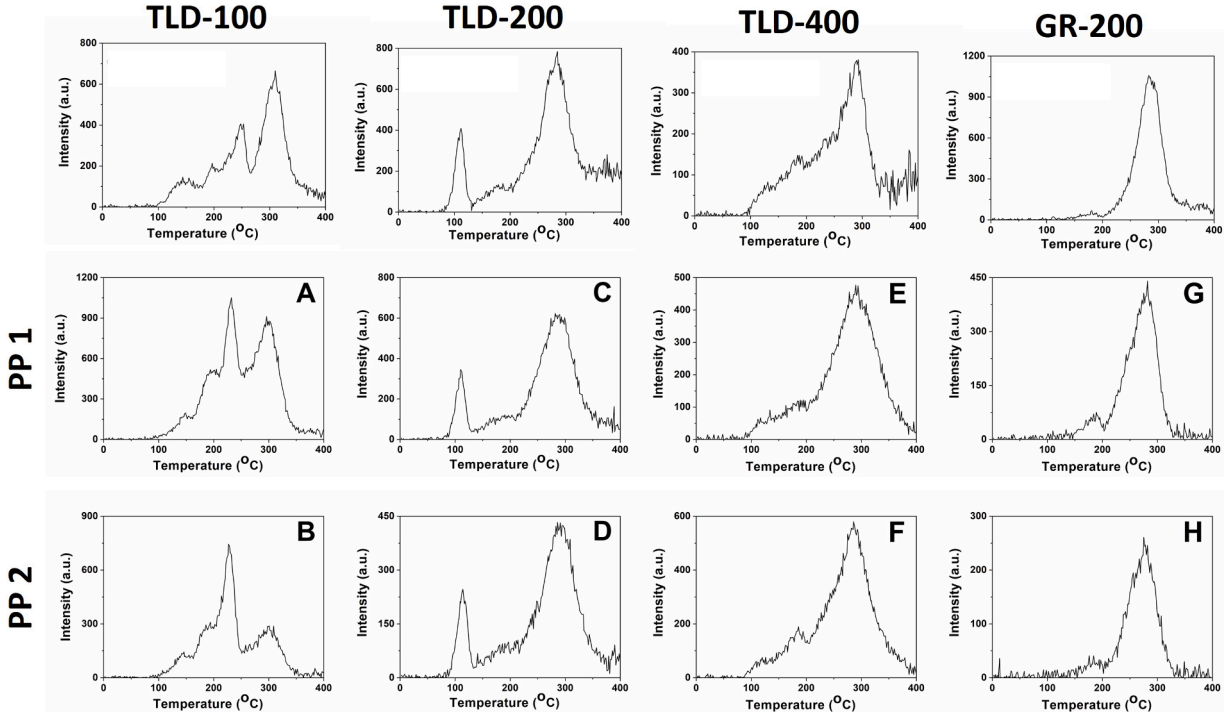


**Fig. 4.** Comparative study of UVC-TL emissions, where: the 1st line represents the dosimeters without PP samples [23] and the 2nd and 3rd lines corresponds to PP 1 (0.20 mm) and PP 2 (0.80 mm), respectively. Additionally, each column illustrates the UVC-TL spectra of commercial dosimeters.

#### 3.4.1. TLD-200 ($CaF_2$: Dy) TL emission study under UVC radiation

In Fig. 4 (c and d), three distinctive constituents of TL emissions induced by UVC radiation are seen in this dosimeter under PP materials. Firstly, a glow emission at ~ 110 °C could imply higher sensitivity to ionizing radiation [23]. Secondly, a TL glow emission between ~ 130 °C to ~ 220 °C, with a peak at around 190 °C, could be due to the non-ionizing part [23]. Conversely, the higher-temperature TL emission, ranging from ~ 230 °C to ~ 350 °C, predominantly corresponds to the ionizing component. These peaks might originate from structural defects and impurities triggered by $Dy^{3+}$ ions (1.59 Å), which are incorporated into $Ca^{2+}$ locations (1.74 Å) in the crystal structure of $CaF_2$ [23].

Upon comparing the ratios of the relative intensity values among these constituents, it is observed that for PP 1 (Fig. 4c) and PP 2 (Fig. 4d) materials, the ratios are 2:1:5 and 2:1:4, respectively. Also, it is important to observe that two varied thicknesses of the samples employed in this investigation, 0.20 mm and 0.80 mm, do not lead to temperature oscillations between ~ 130 °C to ~ 220 °C connected to the non-ionizing part. Nonetheless, apparent disparities emerge in the ionizing part of the UVC-TL emission that is found at ~ 280 °C. Despite the presence of this phenomenon in both samples, the thin PP 1 sample (0.20 mm thickness) has its ionizing component increased. The difference in results may be ascribed to the capability of the PP materials to transmit the ionizing component. As a result, this commercial dosimeter proves ineffective in detecting UVC radiation, exhibiting behavior similar to the one without a plastic sample (2:1:4) in regard to both curve configuration and the correlation of intensities.

#### 3.4.2. TLD-400 ($CaF_2$: Mn) TL emission study under UVC radiation

It can be observed from the TL signal induced by UVC radiation of this commercial dosimeter that there are two distinct groups of components shown in Fig. 4 (E and F) under PP samples. Firstly, a large amount of TL emission was also noticed, reaching up to approximately 200 °C, with the maximum peaking at ~ 190 °C. The more likely explanation is that these emissions may come from the non-ionizing part, in addition to $Mn^{2+}$ impurities (1.17 Å) and defects within the $Ca^{2+}$ locations (1.74 Å) present in the crystal structure of $CaF_2$ [44]. Secondly, a broad peak centered at ~ 290 °C, could be associated with the ionizing part of the UVC radiation. For PP 1 (Fig. 4e) and PP 2 (Fig. 4f) materials, the signal originated from the TLD-400 dosimeter and depicted ratios of relative intensity values, specifically 1:4 and 1:3, respectively. These ratios indicate the presence of two discernible component groups around 190 °C and 290 °C.

Remarkably, the thickness of the samples (0.20 mm and 0.80 mm) has minimal effect on their UVC response, as evidenced by their parallel reaction to UVC radiation up to about 200 °C. This implies that both samples have a similar potential for transmitting UVC light. However, observable distinctions arise in the ionization part of the UVC-induced TL glow peak (peaking at ~ 290 °C), which reveal an enhanced response in the PP sample of lesser thickness (PP 1, 0.20 mm thickness), despite its presence in both film samples. One reason for this difference is that the PP samples may facilitate the transmission of the ionizing part of UVC light. Hence, this commercial dosimeter can be regarded as an unsuitable UVC detector because it exhibits similar response patterns to those found with or without a plastic sample (1:4) but in varying intensity relationships and curve shapes.

#### 3.4.3. GR-200 (LiF: Mg, Cu, P) TL emission study under UVC radiation

The GR-200 dosimeter, represented in Fig. 4 (G and H), exhibits the most significant peak at approximately 280 °C, which belongs to the ionizing part of UVC radiation. Such emission can result from the recombination of crystal defects, including color centers (H-F) and $V_k$−e centres (electron traps and vacancies) [45]. The sensitivity towards the ionizing component of UVC radiation increases with growing temperatures, reaching around 280 °C, whereas a diminished TL signal is observed for low temperatures in the range around 190 °C. The reason described above suggests that GR-200 can be a potential dosimeter for detecting ionizing radiation, but its inability to differentiate between ionizing and non-ionizing components of UVC radiation [23]. Both PP 1 (Fig. 4g) and PP 2 (Fig. 4h) samples show a similar trend, with an intensity ratio of 1:7 and 1:8 respectively, for two major signals peaked at around 190 °C and 280 °C (associated with the ionizing part).

## 4. Conclusions

This study investigates the application of UVC radiation to extend the lifetime healthcare materials containing PP, particularly in PPE items. However, implementing this approach presents significant challenges and considerations. Factors such as, the diverse physical and chemical properties of PP, the need for consistent UVC exposure, and the potential impact of repeated disinfection cycles on the integrity of the materials underline the complexity of this issue. Furthermore, the adoption of such disinfection protocols requires stringent safety measures to mitigate the risks of UVC exposure to healthcare professionals and patients, in addition to considerations for the financial and operational aspects of deploying UVC disinfection systems. Despite these challenges, the opportunity to significantly reduce plastic pollution through the prolonged use of PPE items in healthcare presents a strong rationale for further research and development in this field.

Main objectives involved assessing possible PP damage due to UVC exposure and detecting the presence of UVC radiation using TLDs positioned under PP samples. Findings demonstrate that UVC radiation penetrates PP samples irrespective of their thickness; nevertheless, penetration effectiveness may vary, requiring meticulous assessments in healthcare sectors. This is essential for optimizing UVC treatment protocols to efficiently prolong the lifetime of PPE items.

ATR-FTIR and Raman spectroscopy reveal no degradation in PP samples after UVC irradiation. ATR-FTIR spectra show subtle alterations in characteristic bands, including broadening of the O–H region, potential breakage of C–H bonds impacting $CH_2$ and $CH_3$ stretching bands, changes in the carbonyl (C=O) region suggesting diverse functional groups, modifications in C–H bending vibrations bands and UVC-induced effects on crystalline structure. These changes signify minimal impact from a *photo-oxidative degradation* process on molecular structure (< 7 % for PP 1 and < 4 % for PP 2 relative transmittance). Moreover, Raman spectra indicate resistance to further degradation, with a slight reduction in peak intensity for both PP samples. PP 1 exhibits minor structural changes (< 4 %) with increased $CH_3$ asymmetric bending and $CH_2$ bending vibrations, and PP 2 shows negligible changes (< 1 %), suggesting no apparent polymer chain degradation from UVC exposure. Thus, observed variations might arise from intrinsic PP properties (i.e., polymer molecular mass distribution, crystalline structure and additives) or individual histories (i.e., manufacturing processes and previous environmental contact), instead of being exclusively ascribed to UVC irradiation. Consequently, PP materials exhibit resilience post-UVC irradiation under experimental conditions. Additionally, the comparative study of UVC-TL emissions offers insights into several TLDs materials employed for the detection of UVC radiation. Thus, TLD-100 could serve as a prospective UVC detector with a signal at around 300 °C, due to the non-ionizing part of UVC radiation. Conversely, TLD-200 and TLD-400 do not prove to be effective detectors due to their analogous behavior to that of each dosimeter without a plastic sample, regarding both intensity relationships and curve shape. And the GR-200 lacks the ability to distinguish ionizing and non-ionizing part of UVC radiation. These observations, evident in each PP samples, but especially noticeable in the thinner PP, emphasize the significance of sample thickness is crucial for precise interpretation and detection.

Consistent detection of radiation in PP materials after 1-hour exposure advances understanding of the role of UVC radiation in extending the lifetime of healthcare materials containing PP. These comprehensive insights emphasize the requirement for customized UVC treatment protocols, adaptable to diverse PP thicknesses for ensuring the safety and quality of recycled PPE items. Ultimately, this study showcases UVC

radiation as a possible approach to prolong the lifetime of PP materials, making a substantial contribution to reducing plastic pollution in healthcare sectors.

## Funding

This research did not receive any specific grant from funding agencies in the public, commercial, or not-for-profit sectors.

## Declaration of competing interest

The authors declare that they have no known competing financial interests or personal relationships that could have appeared to influence the work reported in this paper.

## Acknowledgments

Cecilia Boronat would like to thank for the predoctoral researcher contract with UNED-SANTANDER, affiliated with the UNESCO Chair, and for the assistance provided through the program "*UNESCO Chair on Science and Innovation for Sustainable Development: Global Food Production and Safety*".

## References

[1] G. Kannan, B. Mghili, G.E. De-la-Torre, P. Kolandhasamy, M. Machendiranathan, M.V. Rajeswari, A. Saravanakumar, Personal protective equipment (PPE) pollution driven by COVID-19 pandemic in Marina Beach, the longest urban beach in Asia: abundance, distribution, and analytical characterization, Mar. Pollut. Bull. 186 (2023) 114476, https://doi.org/10.1016/j.marpolbul.2022.114476.

[2] M. Hasan, A.R.M.T. Islam, M.M.M.F. Jion, M.N. Rahman, S.D. Peu, A. Das, A.B.M. M. Bari, M.S. Islam, S.C. Pal, A. Islam, T.R. Choudhury, M.R.J. Rakib, A.M. Idris, G. Malafaia, Personal protective equipment-derived pollution during Covid-19 era: a critical review of ecotoxicology impacts, intervention strategies, and future challenges, Sci. Total Environ. 887 (2023) 164164, https://doi.org/10.1016/j.scitotenv.2023.164164.

[3] T.A. Aragaw, Surgical face masks as a potential source for microplastic pollution in the COVID-19 scenario, Mar. Pollut. Bull. 159 (2020) 111517, https://doi.org/10.1016/j.marpolbul.2020.111517.

[4] D. Silva, R. Rocha, C.J. Silva, H. Barroso, J. Botelho, V. Machado, J.J. Mendes, J. Oliveira, M.V. Loureiro, A.C. Marques, E. Alves, A.P. Serro, Gamma radiation for sterilization of textile based materials for personal protective equipment, Polym. Degrad. Stab. 194 (2021) 109750, https://doi.org/10.1016/j.polymdegradstab.2021.109750.

[5] T. Dargaville, K. Spann, M. Celina, Opinion to address the personal protective equipment shortage in the global community during the COVID-19 outbreak, Polym. Degrad. Stab. 176 (2020) 109162, https://doi.org/10.1016/j.polymdegradstab.2020.109162.

[6] C. Boronat, V. Correcher, J. García-Guinea, J.C. Bravo-Yagüe, Effects of UVC irradiation on polystyrene for healthcare packaging: study by FTIR and Raman spectroscopy with thermoluminescence, Polym. Degrad. Stab. 222 (2024) 110700, https://doi.org/10.1016/j.polymdegradstab.2024.110700.

[7] Z. Zhao, Z. Zhang, M. Lanzarini-Lopes, S. Sinha, H. Rho, P. Herckes, P. Westerhoff, Germicidal Ultraviolet Light Does Not Damage or Impede Performance of N95 Masks upon Multiple Uses, Environ. Sci. Technol. Lett. 7 (8) (2020) 600–605, https://doi.org/10.1021/acs.estlett.0c00416.

[8] V.R. Sastri, Commodity Thermoplastics: polyvinyl Chloride, Polyolefins, Cycloolefins and Polystyrene, Plastics in Medical Devices (2022) 113–166, https://doi.org/10.1016/b978-0-323-85126-8.00002-3.

[9] T. Sathish, R. Saravanan, K. Sharma, S. Zahmatkesh, K. Muthukumar, H. Panchal, A novel investigations on medical and non-medical mask performance with influence of marine waste microplastics (polypropylene), Mar. Pollut. Bull. 192 (2023) 115004, https://doi.org/10.1016/j.marpolbul.2023.115004.

[10] R. Lenz, K. Enders, C.A. Stedmon, D.M.A. MacKenzie, T.G. Nielsen, A critical assessment of visual identification of marine microplastic using Raman spectroscopy for analysis improvement, Mar. Pollut. Bull. 100 (1) (2015) 82–91, https://doi.org/10.1016/j.marpolbul.2015.09.026.

[11] A.P. Periyasamy, A. Tehrani-Bagha, A review on microplastic emission from textile materials and its reduction techniques, Polym. Degrad. Stab. 199 (2022) 109901, https://doi.org/10.1016/j.polymdegradstab.2022.109901.

[12] C.C. Ontiveros, D.C. Shoults, S. MacIsaac, K.D. Rauch, C.L. Sweeney, A.K. Stoddart, G.A. Gagnon, Specificity of UV-C LED disinfection efficacy for three N95 respirators, Sci. Rep. 11 (2021) 15350, https://doi.org/10.1038/s41598-021-94810-4.

[13] National Center for Immunization and Respiratory Diseases (U.S.). Division of Viral Diseases., 2020. Decontamination and reuse of filtering facepiece respirators. https://stacks.cdc.gov/view/cdc/90574 (accessed 4 March 2024).

[14] D. Mills, D.A. Harnish, C. Lawrence, M. Sandoval-Powers, B.K. Heimbuch, Ultraviolet germicidal irradiation of influenza-contaminated N95 filtering facepiece respirators, Am. J. Infect. Control. 46 (7) (2018) E49–E55, https://doi.org/10.1016/j.ajic.2018.02.018.

[15] E.M. Fisher, R.E. Shaffer, A method to determine the available UV-C dose for the decontamination of filtering facepiece respirators, J. Appl. Microbiol. 110 (1) (2011) 287–295, https://doi.org/10.1111/j.1365-2672.2010.04881.x.

[16] A.L. Andrady, A.M. Heikkilä, K.K. Pandey, L.S. Bruckman, C.C. White, M. Zhu, L. Zhu, Effects of UV radiation on natural and synthetic materials, Photochem. Photobiol. Sci. 22 (2023) 1177–1202, https://doi.org/10.1007/s43630-023-00377-6.

[17] M.B. Hossain, J. Yu, A.A.U. Nur, P. Banik, Y.N. Jolly, M.Al Mamun, B.A. Paray, T. Arai, Distribution, characterization and contamination risk assessment of microplastics in the sediment from the world's top sediment-laden estuary, J. Environ. Manage. 344 (2023) 118472, https://doi.org/10.1016/j.jenvman.2023.118472.

[18] H. Wu, Y. Zhao, X. Dong, L. Su, K. Wang, D. Wang, Probing into the microstructural evolution of isotactic polypropylene during photo-oxidation degradation, Polym. Degrad. Stab. 183 (2021) 109434, https://doi.org/10.1016/j.polymdegradstab.2020.109434.

[19] G. Socrates, Infrared and Raman characteristic Group Frequencies, Tables and charts, 2001.

[20] D.L. Poster, M. Hardwick, C.C. Miller, M.A. Riley, W.W.S.I. Rodrigo, A.E. Vladar, J. D. Wright, C.D. Zangmeister, C. Zarobila, J. Starkweather, J. Wynne, J. Yilzarde, Disinfection of Respirators with Ultraviolet Radiation, J. Res. Natl. Inst. Stand. Technol. 126 (2021) 126058, https://doi.org/10.6028/jres.126.058.

[21] V. Correcher, C. Boronat, M.D. Virgos, J. Garcia-Guinea, UV-Induced Thermoluminescence of Natural Ca-Rich Carbonates, J. Appl. Spectrosc. 86 (2020) 1004–1009, https://doi.org/10.1007/s10812-020-00931-5.

[22] V. Correcher, J. Garcia-Guinea, Application of the EN 1788 European standard for the control of saffron, pepper and blends, Food Control 22 (2) (2011) 173–179, https://doi.org/10.1016/j.foodcont.2010.05.020.

[23] C. Boronat, V. Correcher, J.C. Bravo-Yagüe, I. Sarasola-Martin, J. Garcia-Guinea, J. F. Benavente, Comparing the effect of electron beam, beta and ultraviolet C exposure on the luminescence emission of commercial dosimeters, Spectrochim. Acta, A Mol. Spectrosc. 295 (2023) 122571, https://doi.org/10.1016/J.SAA.2023.122571.

[24] S.W.S. McKeever, Mechanisms of thermoluminescence production in materials for radiation dosimetry, Radiat. Prot. Dosimetry. 17 (1−4) (1986) 431–435, https://doi.org/10.1093/oxfordjournals.rpd.a079854.

[25] A. Delgado, V. Unamuno, J.L. Muñiz, V. Correcher, J.M. Gómez Ros, A simple UV irradiator for low dose reassessment with LiF TLD-100, Radiat. Prot. Dosimetry. 67 (4) (1996) 303–306, https://doi.org/10.1093/oxfordjournals.rpd.a031834.

[26] L. Bøtter-Jensen, G.A.T. Duller, A new system for measuring optically stimulated luminescence from quartz samples, Int. J. Radiat. Appl. Instrum., Part A, Appl. Radiat. Isot. 20 (4) (1992) 549–553, https://doi.org/10.1016/1359-0189(92)90003-E.

[27] V. Correcher, A. Delgado, On the use of natural quartz as transfer dosemeter in retrospective dosimetry, Radiat. Meas. 29 (3−4) (1998) 411–414, https://doi.org/10.1016/S1350-4487(98)00040-7.

[28] S.N. Tripathi, D.K. Shukla, S. Bonda, S. Saha, A.P. Patade, V.K. Srivastava, G.S. S. Rao, R. Jasra, Investigation of colored lump formation inside the silos during the production of polypropylene copolymer, Polym. Bull. 79 (2022) 11285–11299, https://doi.org/10.1007/s00289-022-04090-9.

[29] E. Yousif, R. Haddad, Photodegradation and photostabilization of polymers, especially polystyrene: review, Springerplus. 2 (2013) 398, https://doi.org/10.1186/2193-1801-2-398.

[30] H. Qin, S. Zhang, H. Liu, S. Xie, M. Yang, D. Shen, Photo-oxidative degradation of polypropylene/montmorillonite nanocomposites, Polymer. (Guildf) 46 (9) (2005) 3149–3156, https://doi.org/10.1016/j.polymer.2005.01.087.

[31] P.V. Joseph, M.S. Rabello, L.H.C. Mattoso, K. Joseph, S. Thomas, Environmental effects on the degradation behaviour of sisal fibre reinforced polypropylene composites, Compos. Sci. Technol. 62 (10−11) (2002) 1357–1372, https://doi.org/10.1016/S0266-3538(02)00080-5.

[32] A.P. Kumar, D. Depan, N. Singh Tomer, R.P. Singh, Nanoscale particles for polymer degradation and stabilization-Trends and future perspectives, Prog. Polym. Sci. 34 (6) (2009) 479–515, https://doi.org/10.1016/j.progpolymsci.2009.01.002.

[33] K.G. De Castro Monsores, A.O. Da Silva, S. De Sant' Ana Oliveira, R.P. Weber, P. F. Filho, S.N. Monteiro, Influence of ultraviolet radiation on polystyrene, J. Mater. Res. Technol. 13 (2021) 359–365, https://doi.org/10.1016/j.jmrt.2021.04.035.

[34] E. Andreassen, Infrared and Raman spectroscopy of polypropylene, Polymer Science and Technology Series 2 (1999) 320–328, https://doi.org/10.1007/978-94-011-4421-6_46.

[35] M. Arruebarrena de Báez, P.J. Hendra, M. Judkins, The Raman spectra of oriented isotactic polypropylene, Spectrochim. Acta, A Mol. Spectrosc. 51 (12) (1995) 2117–2124, https://doi.org/10.1016/0584-8539(95)01512-1.

[36] R. Caban, FTIR-ATR spectroscopic, thermal and microstructural studies on polypropylene-glass fiber composites, J. Mol. Struct. 1264 (2022) 133181, https://doi.org/10.1016/j.molstruc.2022.133181.

[37] B.C. Smith, The infrared spectra of polymers III: hydrocarbon polymers, Spectroscopy 36 (11) (2021) 22–25, https://doi.org/10.56530/spectroscopy.mh7872q7.

[38] J. Fang, L. Zhang, D. Sutton, X. Wang, T. Lin, Needleless melt-electrospinning of polypropylene nanofibres, J. Nanomater. (2012) 382639, https://doi.org/10.1155/2012/382639, 2012.

[39] K.D. Dahm, D.J. Dahm, Theoretical models of light scattering and absorption, Near-Infrared Spectros. Near-Infrared Spectros (2021) 37–60, https://doi.org/10.1007/978-981-15-8648-4_3.
[40] Smith, E., Dent, G., 2019. Modern Raman Spectroscopy – A Practical Approach. https://doi.org/10.1002/0470011831.
[41] B.H. Stuart, Polymer crystallinity studied using Raman spectroscopy, Vib. Spectrosc. 10 (2) (1996) 79–87, https://doi.org/10.1016/0924-2031(95)00042-9.
[42] J.S. Dryden, B. Shuter, The dependence of the thermoluminescence of LiF: $mg^{2+}$ crystals on the state of aggregation of the $Mg^{2+}$ ions, J. Phys. D. 6 (1) (1973) 123, https://doi.org/10.1088/0022-3727/6/1/316.
[43] D. Weiss, Y.S. Horowitz, L. Oster, Delocalized recombination kinetic modeling of the LiF:mg,Ti (TLD-100) glow peak 5 TL system, Radiat. Meas. 43 (2−6) (2008) 254–258, https://doi.org/10.1016/j.radmeas.2007.10.026.
[44] M. Topaksu, V. Correcher, J. Garcia-Guinea, Luminescence emission of natural fluorite and synthetic $CaF_2$: mn (TLD-400), Radiat. Phys. Chem. 119 (2016) 151–156, https://doi.org/10.1016/j.radphyschem.2015.10.002.
[45] B. Yang, L. Wang, P.D. Townsend, H. Gao, Comparison between the low temperature thermoluminescence spectra in annealed LiF:mg,Cu, LiF:mg,Cu,P and LiF:mg,Cu,Si, Nucl. Instrum. Methods Phys. Res. B. 266 (11) (2008) 2581–2586, https://doi.org/10.1016/j.nimb.2008.03.199.